Accepted Manuscript

A Novel Nanocomposite with Superior Electrocatalytic Activity: A Magnetic Property Based $ZnFe_2O_4$ Nanocubes Embellished with Reduced Graphene Oxide by Facile Ultrasonic Approach

Tse-Wei Chen, Umamaheswari Rajaji, Shen-Ming Chen, Muneerah Mogren Al Mogren, Majdi Hochlaf, Sarah Dhaif Allah Al Harbi, R. Jothi Ramalingam

PII: S1350-4177(19)30280-9
DOI: https://doi.org/10.1016/j.ultsonch.2019.05.007
Reference: ULTSON 4590

To appear in: *Ultrasonics Sonochemistry*

Received Date: 21 February 2019
Revised Date: 6 May 2019
Accepted Date: 7 May 2019

Please cite this article as: T-W. Chen, U. Rajaji, S-M. Chen, M.M.A. Mogren, M. Hochlaf, S.D.A. Harbi, R.J. Ramalingam, A Novel Nanocomposite with Superior Electrocatalytic Activity: A Magnetic Property Based $ZnFe_2O_4$ Nanocubes Embellished with Reduced Graphene Oxide by Facile Ultrasonic Approach, *Ultrasonics Sonochemistry* (2019), doi: https://doi.org/10.1016/j.ultsonch.2019.05.007

A Novel Nanocomposite with Superior Electrocatalytic Activity: A Magnetic Property Based $ZnFe_2O_4$ Nanocubes Embellished with Reduced Graphene Oxide by Facile Ultrasonic Approach

Tse-Wei Chen[a,b,‡], Umamaheswari Rajaji[a, ‡], Shen-Ming Chen[a,], Muneerah Mogren Al Mogren[c], Majdi Hochlaf[d], Sarah Dhaif Allah Al Harbi[c], R. Jothi Ramalingam[e]*

[a]Department of Chemical Engineering and Biotechnology, National Taipei University of Technology, No.1, Section 3, Chung-Hsiao East Road, Taipei 106, Taiwan

[b]Research and Development Center for Smart Textile Technology, National Taipei University of Technology, No.1, Section 3, Chung-Hsiao East Road, Taipei 106, Taiwan

[c]Chemistry Department, Faculty of Science, King Saud University, P.O. Box 2455, Riyadh 11451, Kingdom of Saudi Arabia

[d]Laboratoire Modelisation et Simulation Multi Echelle, MSME UMR 8208 CNRS, University Paris-Est, ´5 Blvd. Descartes, 77454 Marne-la-Vallee, France

[e]Surfactant Research Chair, Chemistry Department, College of Science, King Saud University, P.O. Box-2455, Riyadh-11451, Kingdom of Saudi Arabia

Corresponding author: Email: smchen78@ms15.hinet.net, (S.-M. Chen) ‡-equal contribution.

Abstract

Herein, a novel Zinc Ferrite nanocubes ($ZnFe_2O_4$ NCs) decorated reduced graphene oxide (rGO) nanocomposite have been designed through a sonochemical method. After then, as-synthesized $ZnFe_2O_4$ NCs/rGO was characterized by XPS, XRD, HRTEM and EIS. Furthermore, the $ZnFe_2O_4$ NCs/rGO nanocomposite modified GCE (galssy carbon electrode) shows excellent electrochemical sensing performance towards biomarker of 4-nitroquinoline N-oxide (4-NQ) with fast detection. 4-NQ is one of the important cancer biomarker. Moreover, the fabricated sensor showed a wide linear window for 4-NQ between 0.025-534.12 µM and nanomolar detection limit (8.27 nM). Further, the as-prepared $ZnFe_2O_4$ NCs/rGO/GCE has been applied to the determination of 4-NQ in human blood and urine samples with excellent recovery results.

Keywords: Zinc Ferrite; 4-nitroquinoline N-oxide; Toxic chemical detection, Reduced graphene oxide; Biological samples.

1. Introduction

Zinc ferrite ($ZnFe_2O_4$), a common transition bimetal oxide, has been widely utilized as an electro-catalyst to prepare highly effective nanocomposite for the electrochemical applications such as water splitting, supercapacitors, batteries, electro and photocatalysis, due to their unique structural properties, including ordered crystal structure, large surface area and stability [1-8]. Since, it has used various applications and various fields [9-14]. Although, few studies have focused on using zinc ferrites based nanocomposites as novel modified electrode

materials due to their aggregation. In this aspect, integrating zinc ferrites and high conductive nanomatrix into nanocomposites have been developing as a precious approach to improve the non-aggregativity and conductivity of the electrocatalyst [15-21].Furthermore, various nano-layers matrix as a graphene based high conductive nanomaterials have been widely applied to establish with zinc ferrites to improve their electrochemical performances [22, 23]. The reduced graphene oxide (rGO) is one of the novel layered nanomaterial that possess good conductivity, large electrocatalytic surface area and porosity [24-27]. Therefore, we can focused the synthesis of zinc ferrites ($ZnFe_2O_4$) decorated reduced graphene oxide based nanocomposite is considered as an effective way to enhance the electrochemical sensing performances towards the biomarker application.

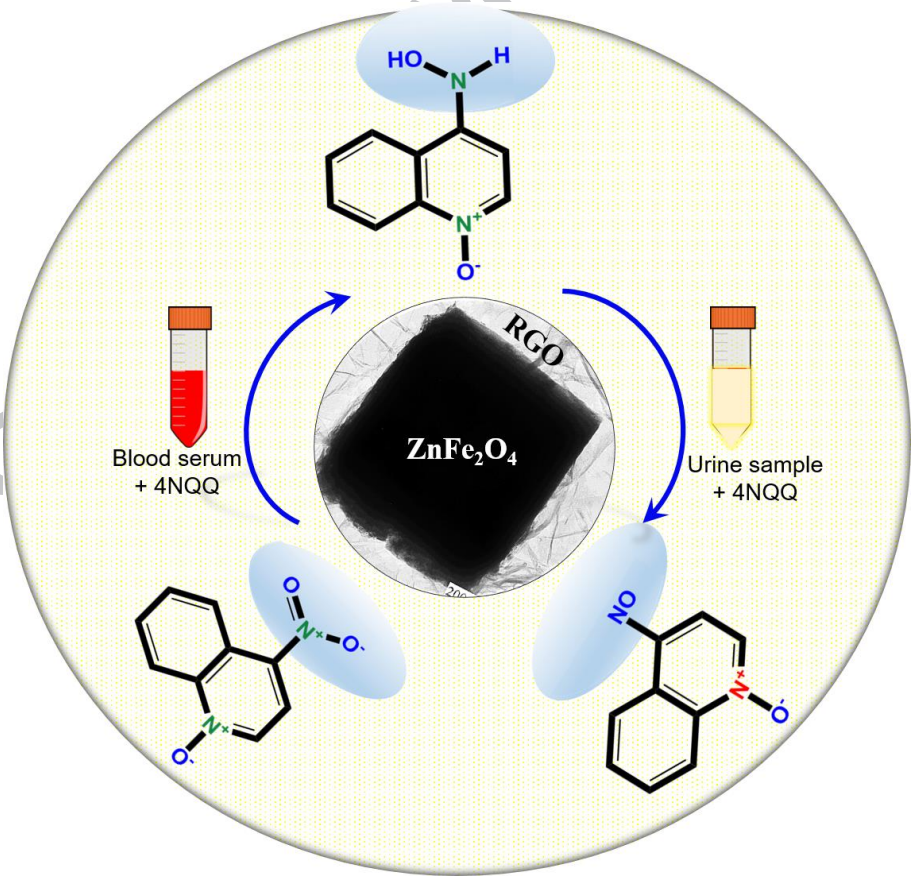

Scheme 1. Schematic diagram of the work

Cancer is an important disease in human life that has become a serious and increasing global health problem. Moreover, 4-nitroquinoline N-oxide (4-NQ) has considerable research attention due to tumorigenic properties and 4-NQ is one of the toxic biomarker in cancer research and which is find from the tumorigenic part or cells [28]. When increase the oxidative stress and DNA mutations in the human body, it has produced to 4-NQ biomarker [28]. In addition, 4-NQ is induced cancer-causing DNA mutations [28-30]. Since, when increasing the concentration of 4-NQ, its causing high carcinogenesis effect in the human system such as mutagenicity and genotoxicity [28, 31-33]. Therefore, the determination of 4-NQ marker in various biological system is of highly great potential for analytical and research applications. Moreover, few detection methods are reported such as microbial assay, high-performance liquid chromatography-MC (HPLC) and electron paramagnetic resonance spectrometry [34-36]. Moreover, these methods are expensive and long-time process. Nevertheless, the electrochemical methods are inexpensive, more efficient and fast than other detection methods [37-44]. Therefore, we can develop the electrochemical sensing method based $ZnFe_2O_4$/rGO nanocomposite in this work for the electrochemical detection of 4-NQ marker.

In this study, reveals that the nanocubes based $ZnFe_2O_4$ nanocatalyst enhance the electrocatalytic and sensing performance towards 4-NQ. Furthermore, to the best of our knowledge, the electrochemical sensing application of $ZnFe_2O_4$/rGO nanocomposite has not been published yet. Moreover, we have synthesized the $ZnFe_2O_4$/rGO nanocatalyst by an ultrasound based sonochemical process. In addition, $ZnFe_2O_4$ based rGO companied nanomaterials that are exhibited the excellent electrochemical sensing properties towards

biomarker. Moreover, $ZnFe_2O_4$ nanocubes decorated carbon nanosheets were successfully synthesized and fabricated using the simple sonochemical approach. In the present work, the synthesized $ZnFe_2O_4$/rGO was fabricated on GCE and characterized. Then the fabricated electrode was used to determination of 4-NQ biomarker in biological samples. Furthermore, the sensitivity of the $ZnFe_2O_4$/rGO nanocomposite modified GCEs were evaluated by electrochemical techniques (**Scheme 1**).

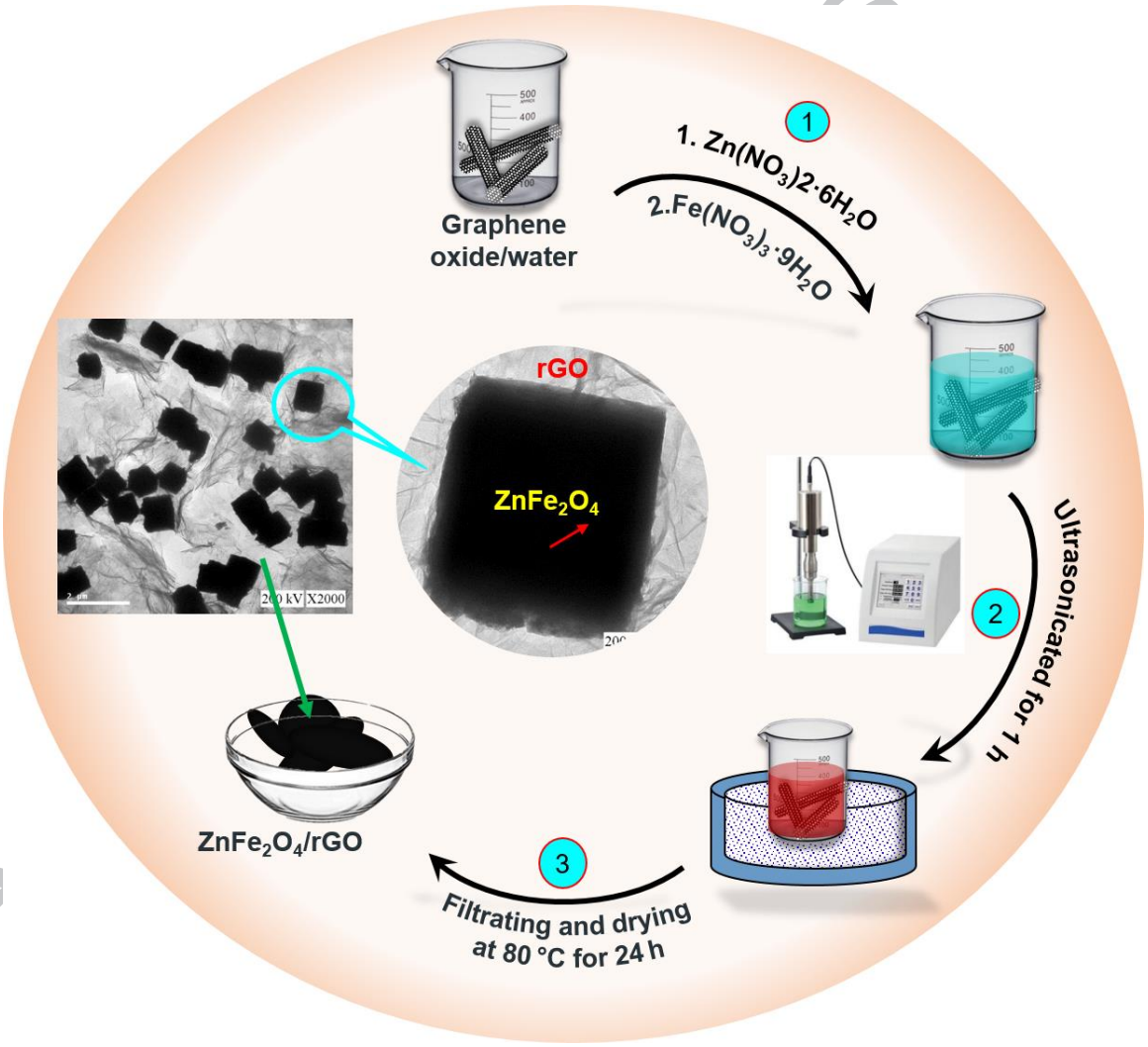

Scheme 2. Facile sonochemical synthesis of $ZnFe_2O_4$/rGO nanocomposite.

2. Experimental section

2.1 Synthesis of $ZnFe_2O_4$ NCs/rGO nanocomposite

All chemicals and reagents were purchased from Sigma-Aldrich with analytical grade and used without any further purification (chemical and methods given in supporting information). A typical synthesized 25 mg of graphene oxide were subsequently added to the pre-prepared mixture solution of 0.2 M ($Zn(NO_3)_2 \cdot 6H_2O$) and 0.4 M ($Fe(NO_3)_3 \cdot 9H_2O$ in 50 mL of deionized water. Then, pH of the prepared suspension was adjusted to 8.0 pH by slowly adding 0.1 M of NH_4OH solution under the stirring and then ultrasonicated for 15 min. After the suspension was sonicated in ultrasonic bath of 100 W at 40 kHz for 1 h. Finally, $ZnFe_2O_4$/rGO nanocomposite was obtained by filtrating and drying at 80°C for 24 h (**Scheme 2**). For controlled experiments, pure $ZnFe_2O_4$ and rGO were also prepared using the procedure described above but without an addition of graphene oxide and metal oxide sources respectively.

2.2. Fabrication of $ZnFe_2O_4$ NCs/rGO modified electrode

The hybrid nanomaterials dispersed solution (2 mg/mL; ethanol) about 8 µL was drop casted on the pre-cleaned electrode surface. Finally, the $ZnFe_2O_4$ NCs/rGO modified electrode was dried in the oven at room temperature. Furthermore, same produce was applied to fabricate for control electrodes such as rGO and $ZnFe_2O_4$ NCs. The fabricated and unmodified electrodes were applied for the electrochemical determination of the 4-NQ.

3. Results and discussion

3.1. Morphological characterization

Evidently, the well-shaped morphologies and uniform nanocube structures are observed in **Figure 1B and C**. and HRTEM image of reduced graphene oxide nanosheets shown in **Figure 1A** and it's like layered multi-carbon nanosheets and reduced nanosheets. As shown in Figure D-E, the rGO nanosheets were comprised of non-aggregated, winkled, highly thin and transparent nanosheets randomly, which agrees well arrangements of the nanocomposite. As HRTEM shows, the nanocubes as structure were obtained for the synthesized $ZnFe_2O_4$ nanoparticles on the sonochemically reduced carbon nanosheets. These results were confirmed that the formation of $ZnFe_2O_4$ NCs/rGO.

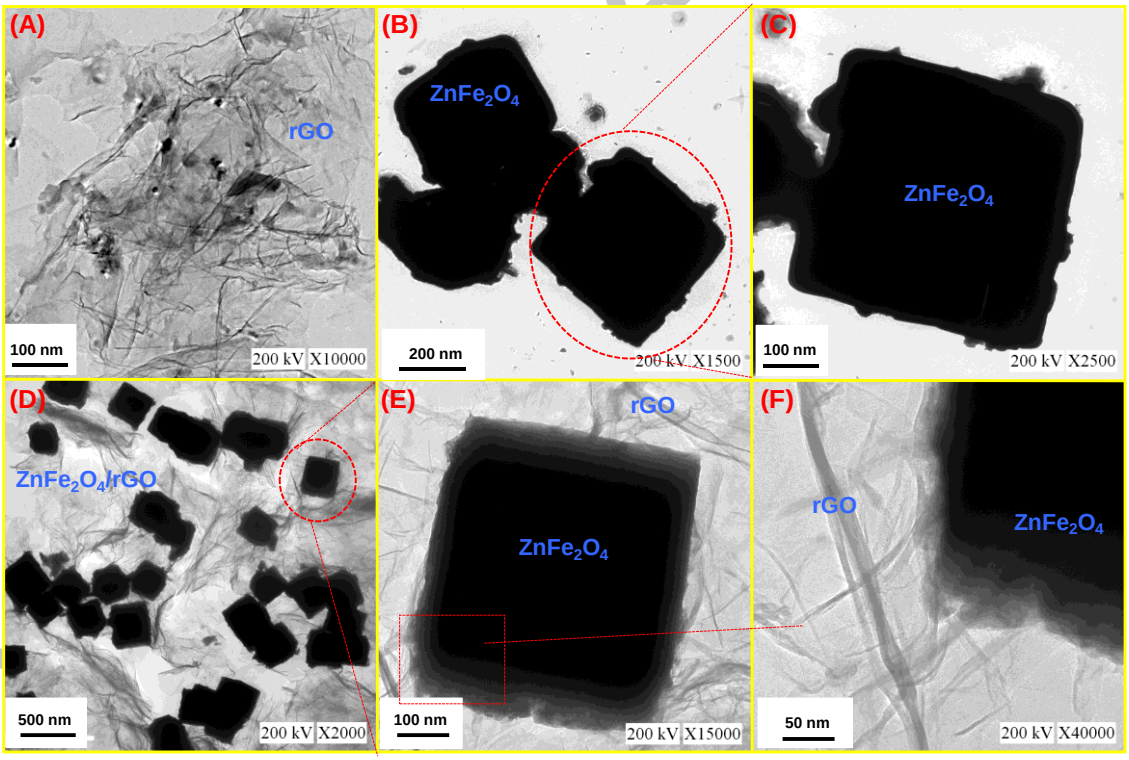

Figure 1. HRTEM images of rGO (A) and $ZnFe_2O_4$ nanocubes (B-C). HRTEM images of $ZnFe_2O_4$ NCs/rGO nanocomposite (D) and high magnification images (E-F).

3.2. XRD and XPS analysis

The XRD patterns of $ZnFe_2O_4$ NCs (blue line) and $ZnFe_2O_4$ NCs/rGO (green line) was displayed in **Figure 2A**. The XRD pattern of the $ZnFe_2O_4$ NCs/rGO shows, several diffraction peaks at 30.08°, 35.64°, 43.32°, 54.28°, 57.26° and 62.16° are observed that are correlated to (220), (311), (400), (422), (511) and (440) crystal planes. This diffraction patterns were matched with the orthorhombic $ZnFe_2O_4$ NCs (**JCPDS No. 22-1012)** [45-47]. Therefore, the XRD pattern indicates the successful formation of $ZnFe_2O_4$ NCs. Besides, the rGO exhibited the diffraction peaks assigned for the miller indices plane is (002). Furthermore, formation of $ZnFe_2O_4$ NCs are evaluated by Figure 2A. Finally, this information is regenerated in the $ZnFe_2O_4$ NCs/rGO confirms the composite formation.

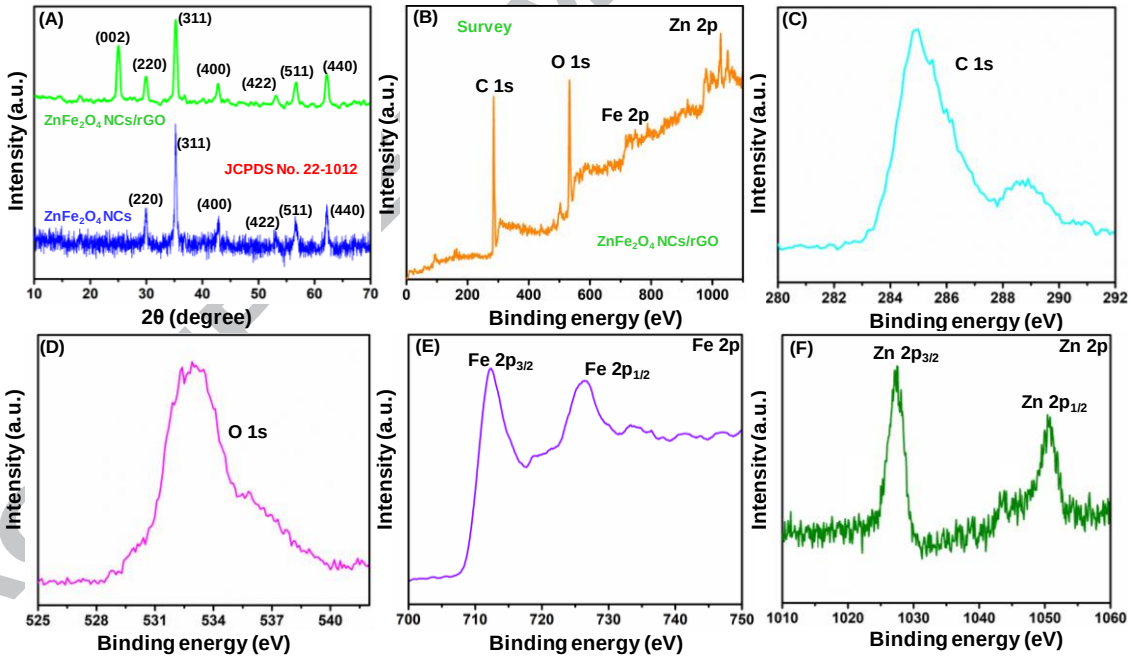

Figure 2. XRD analysis of $ZnFe_2O_4$ NCs and $ZnFe_2O_4$ NCs/rGO (A). XPS survey spectrum of $ZnFe_2O_4$ NCs/rGO (B) and de-conventional peaks of C1s (C), O1s (D), Fe 2p (E) and Zn 2p (F).

X-ray photoelectron spectroscopy (XPS) characterization is one of the specific tool for the evaluation of chemical states and composition of the nanocomposites. The full survey XPS analysis of $ZnFe_2O_4$ NCs/rGO nanocomposites shows in **Figure 2B.** The peak of C 1s O 1s, Fe 2p and Zn 2p were detected in the full scan XPS spectrum. As can be seen that the characteristic peak for C 1s, O 1s, Zn 2p and Fe 2p levels were observed at their correlated binding energies. As shown in **Figure 2C**, the high resolutions scan of the C 1s represents the four major peak due to ring carbon (C-C/-C=C, -C-O, -C=O and -C-C=O). Then **Figure 2D,** the XPS spectrum of the O 1s present in the $ZnFe_2O_4$ NCs/rGO reveals the primary peak denotes the metal-oxygen bonds located. As shown in **Figure 2E**, two dominant peaks of Fe 2p bounded with the metal that exhibited the Fe $2p_{3/2}$ and Fe $2p_{1/2}$ located at the (158.8 eV) and (163.4 eV). In **Figure 2F,** the XPS spectrum of the Zn 2p present in the nanocomposite reveals the two peaks denoted the Zn $2p_{3/2}$ and Zn $2p_{1/2}$ at (1025 to 1055 eV) which demonstrate the Zn present in the form of $ZnFe_2O_4$ NCs/rGO nanocomposite.

3.3. Electrochemical characterization of modified and unmodified electrodes

The electrochemical properties of interfacial electron transport behavior are evaluated by CV [48-50]. The conductivity and interfacial character of bare GCE (a), rGO/GCE (b), $ZnFe_2O_4$ NCs/GCE (c), and $ZnFe_2O_4$ NCs/rGO/GCE (d) were investigated in **Figure 3A and B.** The CV analysis was carried out by 0.1 M KCl containing 5 mM $[Fe(CN)_6]^{-3/-4}$ solution at a fixed scan rate (50 mV/s). In **Figure 3A,** shows the CVs of modified and unmodified electrodes such as bare GCE (a), rGO/GCE (b), $ZnFe_2O_4$ NCs/GCE

(c) and $ZnFe_2O_4$ NCs/rGO/GCE (d). The catalyst modified and unmodified electrodes shows the redox peak, for the comparison the bare GCE, rGO/GCE and $ZnFe_2O_4$ NCs/GCE were low and modulator peak current. Mainly, the nanocomposite modified GCE has higher peak current with low peak potential. In **Figure 3B**, shows that the scan rate of the nanocomposite modified GCE and the results was plot to the corresponding calibration analysis (20 to 300 mV/s). Furthermore, the randles sevcik equation (1) has applied into the slope of the electrochemical analysis in **Figure 3C.** In addition, the electrochemical active surface area of the modified and unmodified electrode as bare GCE, rGO/GCE, $ZnFe_2O_4$ NCs/GCE, and $ZnFe_2O_4$ NCs/rGO/GCE has been calculated as 0.086 cm^2, 0.126 cm^2, 0.158 cm^2 and 0.179 cm^2 respectively. Therefore, the results show that the $ZnFe_2O_4$ NCs/rGO modified GCE is the higher surface area and high conductivity. Due to the properties of rGO and $ZnFe_2O_4$ nanocubes.

$$\mathbf{Ip = 2.69\times10^5 n^{3/2} A D^{1/2} C v^{1/2}} \qquad \mathbf{(1)}$$

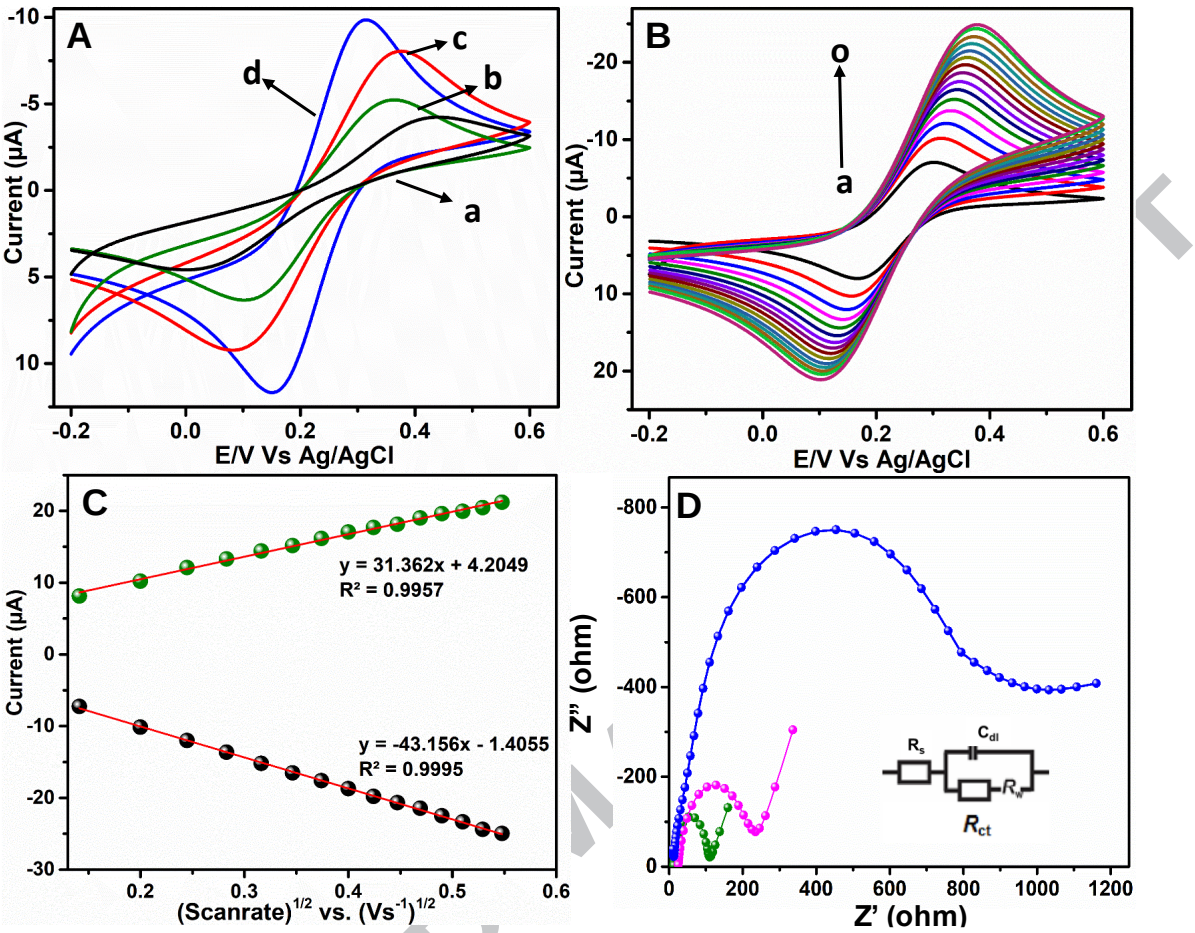

Figure 3. (A) CVs of bare GCE (a), rGO/GCE (b), $ZnFe_2O_4$ NCs/GCE (c) and $ZnFe_2O_4$ NCs/rGO/GCE (d) in 0.1 M KCl containing 5 mM $[Fe(CN)_6]^{-3/-4}$ solution. (B) Scan rate of the nanocomposite modified electrode. (C) Calibration plot of (scan rate vs $Vs^{-1})^{1/2}$. (D) EIS spectra of bare GCE (a), $ZnFe_2O_4$ NCs/GCE (b) and $ZnFe_2O_4$ NCs/rGO/GCE (c).

The electrochemical properties of interfacial electron transport behavior are evaluated by electrochemical impedance spectroscopy (EIS). The Nyquist plot exposed the various modified and unmodified electrodes including bare GCE (a), $ZnFe_2O_4$ NCs/GCE (b) and $ZnFe_2O_4$ NCs/rGO/GCE (c) shown in **(Figure 3A).** The EIS analysis was carried out by 0.1 M KCl containing 5 mM $[Fe(CN)_6]^{-3/-4}$ solution then the frequency ranges of 100 MHz to 100 kHz. The Nyquist plot explained the linear and semicircular, which described the lower and

higher frequencies on the modified and unmodified electrodes. The results were compared with the bare GCE and $ZnFe_2O_4$ NCs/GCE and its depicts the higher semicircular and larger R_{ct} value around 736.48 Ω and 249.62 Ω than $ZnFe_2O_4$ NCs/rGO/GCE. Because, the $ZnFe_2O_4$ NCs/rGO modified GCE shows the small semicircular and low R_{ct} value of 106.25 Ω. Therefore, the nanocomposite has high conductive nanomaterials due to the properties of rGO. Thus, the EIS results also indicated the formation of the nanocomposite with the rGO.

3.4. Electrochemical catalysis of 4-NQ on $ZnFe_2O_4$ NCs/rGO/GCE

The capability of the electrocatalyst modified and unmodified GCE towards the electrochemical sensing of 4-NQ was analyzed by using CV method in **Figure 4**. In **Figure 4A** shows the CV curves of the bare GCE (a), rGO/GCE (b), $ZnFe_2O_4$ NCs/GCE (c) and $ZnFe_2O_4$ NCs/rGO/GCE (d) in 100 µM 4-NQ in 0.05 M PB of pH 7.0. In all electrodes were scanned from a potential of 0.25 V to -0.65 V at a scan rate of 50 mV/s. The poor sensitivity and peak current exhibited by the bare GCE towards reduction reaction of 4-NQ was improved considerably upon modification. Then, the rGO and $ZnFe_2O_4$ NCs modified GCE are moderately improved towards the reduction of 4-NQ. Because, both electrodes have good electrocatalytic ability due to their unique properties. In addition, commercial $ZnFe_2O_4$ nanoparticles modified GCE was checked and it has low peak current compared with sonochemically synthesized $ZnFe_2O_4$ NCs modified GCE (Figure S1). Mainly, the developed $ZnFe_2O_4$ NCs/rGO modified electrode, the reduction peaks current of the 4-NQ enhanced up to 9.21 µA. The enhancement in the electrochemical performance has attributed to the synergistic activity of rGO and $ZnFe_2O_4$ NCs. Moreover, the electrochemical sensing mechanism of 4-NQ is converted into 4-hydroxyaminoquinoline N-oxide are given in **Scheme 3** and then, the 4-hydroxyaminoquinoline N-oxide has converted into 4-

nitrosoquinoline N-oxide (step-2). Higher sensitivity of the $ZnFe_2O_4$ NCs/rGO fabricated electrode were attributed to the fact that the 4-NQ could interact through the conductive electrocatalyst onto the GCE.

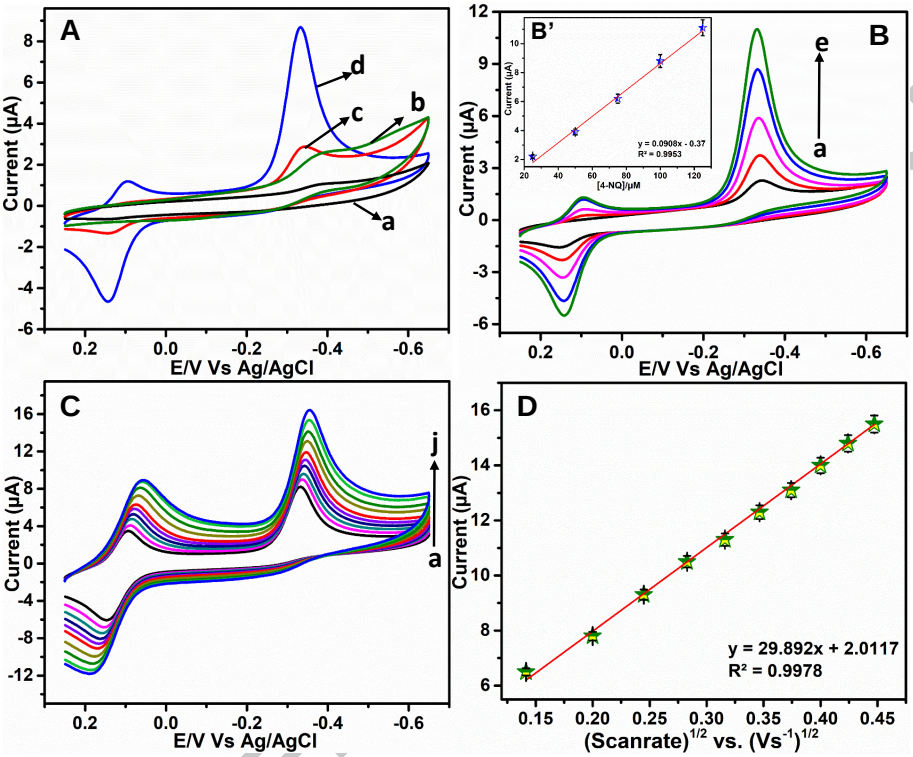

Figure 4. (A) CVs of bare GCE (a), rGO/GCE (b), $ZnFe_2O_4$ NCs/GCE (c) and $ZnFe_2O_4$ NCs/rGO/GCE (d) containing 100 µM 4-NQ in 0.05 M PB (50 mV/s). (B) Various concentration of 4-NQ (25 to 125 µM) and (Inset) shows the plot between 4-NQ concentration versus cathodic peak current. (C) CV curves of different scan rate study ranges from (20 to 200 mV/s) on $ZnFe_2O_4$ NCs/rGO/GCE for the reduction of 100 µM 4-NQ in 0.05 M PB. (D) The calibration plot between the cathodic current (I_{pc}) vs. the square root of the scan rates.

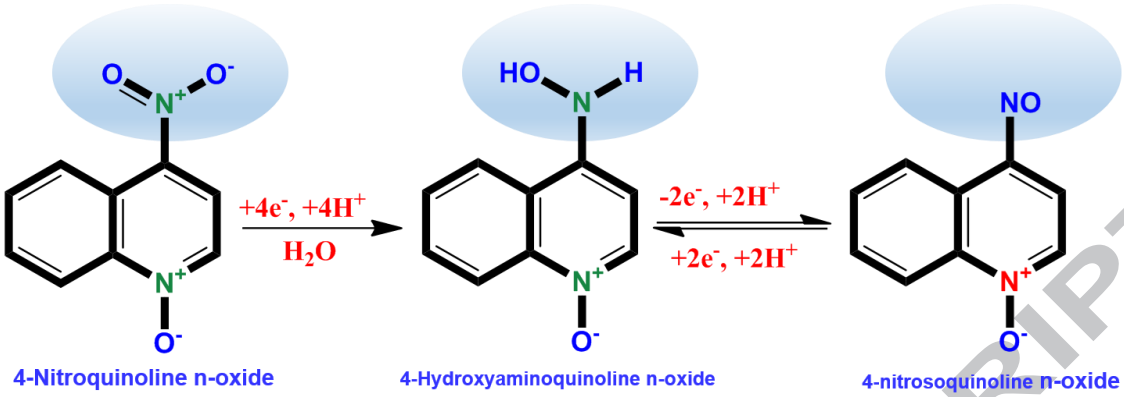

Scheme 3. The electrochemical reduction reaction and mechanism of 4-NQ based on $ZnFe_2O_4$ NCs/rGO modified GCE.

3.5. Effect of concentration, scan rate and pH

Figure 4B, shows the CVs of $ZnFe_2O_4$ NCs/rGO modified electrode in 0.05 M PB containing various concentration of 4-NQ (a to e). When increase the concentration of 4-NQ, a considerable increase in cathodic or reduction peak current. Furthermore, increase the 4-NQ concentration, the cathodic peak current increased linearly. As shown in **Figure 4A** (inset), the cathodic peak currents were increased linearly for the increasing concentration 4-NQ from 25 to 125 µM and the electrochemical reduction linear regression equation y= 0.0908x-0.37 and the correlation co-efficient is calculated as R^2= 0.9953. These result reveals that the nanocompsite modified electrode has great potential to electrochemically reduced the 4-NQ to 4-NQ-NHOH and its evidences proved the good electrochemical performance of the $ZnFe_2O_4$ NCs/rGO/GCE.

The effect of the scan rates (20 to 200 mV/s) were evaluated on $ZnFe_2O_4$ NCs/rGO modified GCE containing 100 µM of 4-NQ in pH 7.0 (**Figure 4C**). Furthermore, the cathodic peak currents were increase with the increasing the scan rates from 20 to 200 mV/s and the obtained cathodic peak currents was plotted with different square root of the scan rates. As

shown in **Figure 5D**, cathodic peak currents are linearly increased with the square root of the scan rates and the correlation coefficient of R^2=0.9978. This results reveals that the electrochemical reduction of 4-NQ at $ZnFe_2O_4$ NCs/rGO/GCE is diffusion controlled process.

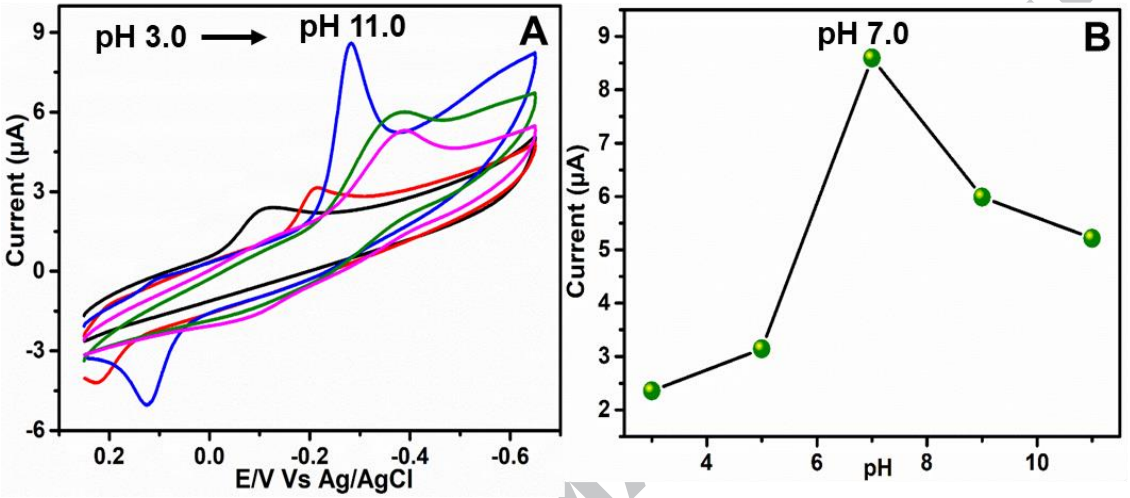

Figure 5. (A) CVs of the $ZnFe_2O_4$ NCs/rGO/GCE in the presence of 100 µM 4-NQ in various pH solutions of (3.0, 5.0, 7.0, 9.0 and 11.0). (B) Plot of pH versus cathodic peak current (I_{pc}).

The effect of pH on the voltammetric detection of 4-NQ with $ZnFe_2O_4$ NCs/rGO modified GCE was examined over various pH ranges from pH 3.0 to 11.0. From **Figure 5A**, it is found that the reduction peak current on the various pH of PB. The calibration plot of pH versus cathodic peak current reveals that, as pH solution changes from lower to higher pH, a peak potential were shift to negative side and it is also observed that the peak current increases with increasing pH. Nevertheless, maximum peak current and response is obtained in pH 7.0 (Figure 5A). Therefore, PB 7.0 is chosen as the optimum pH for the electrochemical determination of 4-NQ on the $ZnFe_2O_4$ NCs/rGO modified GCE.

3.6. Electrochemical determination of 4-NQ by DPV techniques

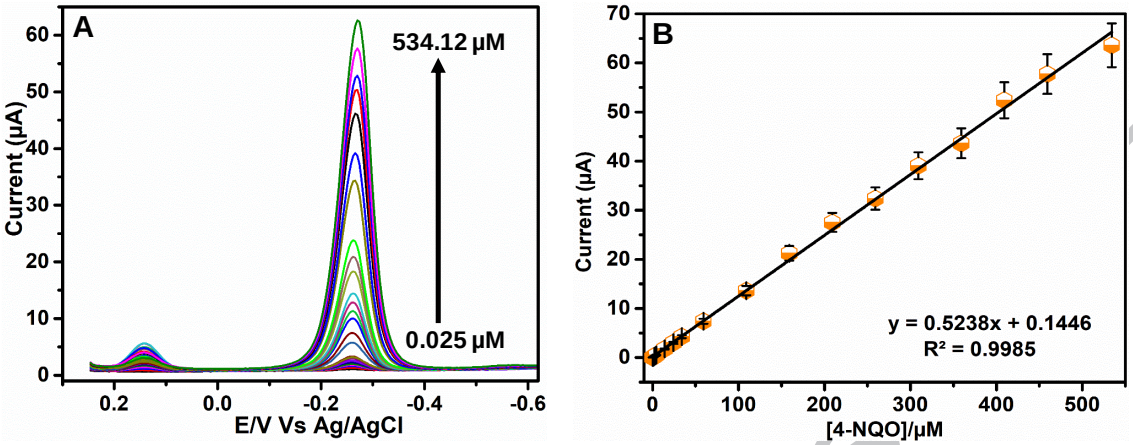

Figure 6. (A-B) DPV responses for the successive additions of 4-NQ in 0.05 M PB (pH 7.0) and various concentration ranges from (0.05 to 574.2 µM) at $ZnFe_2O_4$ NCs/rGO/GCE. (C-D) The linear plot of 4-NQ concentrations versus current response.

The DPV (differential pulse voltammetry) is one of the electrochemical technique and its highly sensitive technique compare then the CV method. Hence, the DPV technique was employed to check the analytical performance of the $ZnFe_2O_4$ NCs/rGO/GCE towards the biomarker of 4-NQ in 0.05 M PB at scan rate 50 mV/s. In **Figure 6A** shows the DPV for the determination of 4-NQ for the different concentrations additions from 0.025 to 534.12 µM. Moreover, **Figure 6B** depicts the corresponding calibration plot between peak current verses concentration of 4-NQ. The electrocatalytic peak current response was increased for each addition of 4-NQ based $ZnFe_2O_4$ NCs/rGO/GCE. Furthermore, the linear regression equation y = 0.5238x +0.1446 with the correlation co-efficient is R^2= 0.9985. Moreover, the peak current responses were increased linearly proportional to the different concentration of 4-NQ. In addition, the linear range was calculated as 0.025 to 534.12 µM and the detection limit is 8.27 nM and sensitivity 7.377 µA μM^{-1} cm^{-2} was observed. Besides, limit of quantification is calculated to be 0.025 µM. These results reveals that the excellent electrochemical

performance of the proposed $ZnFe_2O_4$ NCs/rGO nanomaterials modified GCE for the determination of 4-NQ.

3.7. Selectivity, stability and reproducibility of the sensor

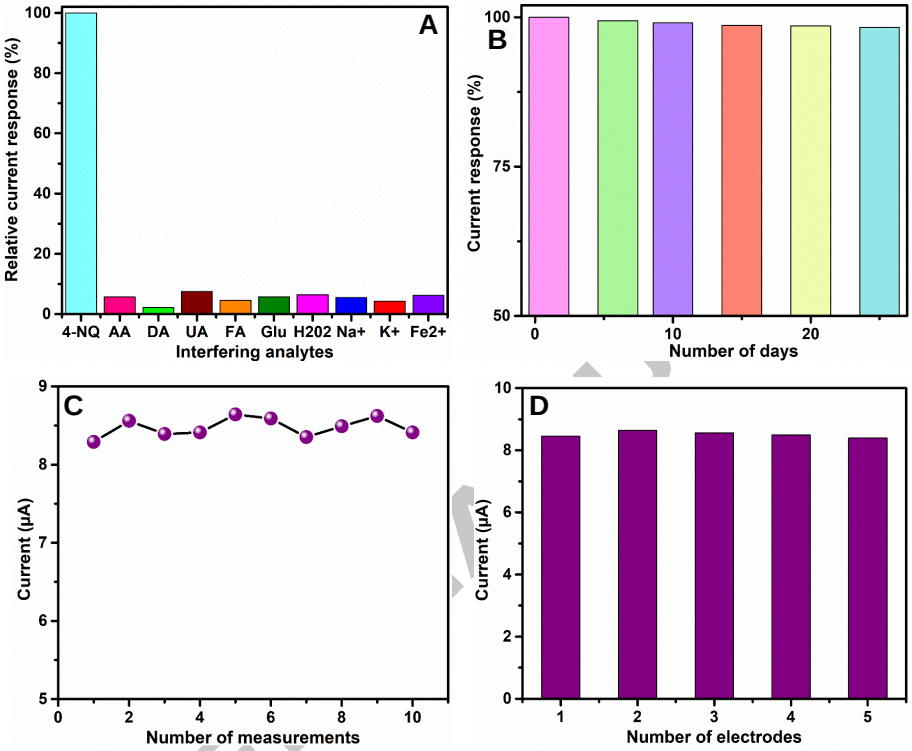

Figure 7. (A) DPV responses of $ZnFe_2O_4$ NCs/rGO/GCE towards 50 µM of 4-NQ with 0.5 mM of interfering compounds. (B) Stability of the sensor as its continuous usage for 25 days containing 100 µM 4-NQ in 0.05 M pH 7.0. (C) Plot for repeatability and (D) reproducibility of $ZnFe_2O_4$ NCs/rGO/GCE containing 100 µM of 4-NQ.

Selectivity is one of the most important parameter for the detection of different biologically important molecules. Hence, we have studied the interference effect for the detection of 4-NQ in presence of some common biomolecules, co-existing and potentially interfering molecules. **Figure 7A.** exhibited the DPV responses for the additions of 0.5 mM of ascorbic acid, dopamine, uric acid, folic acid, glucose, H_2O_2, Na^+, K^+ and Fe^{2+} in presence

of 50 µM of 4-NQ. Moreover, the obtained DPV results reveals that the important biomolecules are not affects much of the 4-NQ response. Therefore, these results are exemplifying the good selectivity of the $ZnFe_2O_4$ NCs/rGO/GCE towards the determination of 4-NQ.

In addition, the stability of the $ZnFe_2O_4$ NCs/rGO/GCE was explored by DPV technique. **Figure 7B** depicts the DPV current response for the addition of 100 µM 4-NQ in 0.05 M PB (pH 7.0) at $ZnFe_2O_4$ NCs/rGO/GCE. The stability study shows that the initial peak current value of the 4-NQ reduction was decreased to only 6.18% over 25 days. For the reproducibility analysis five different $ZnFe_2O_4$ NCs/rGO modified GCE were prepared and the DPV were recorded in presence of 100 µM of 4-NQ with the obtained results RSD were calculated to be 3.57% (**Figure 7D)**. The $ZnFe_2O_4$ NCs/rGO modified electrode was tested for ten times and the RSD value were calculated to be 3.47% (**Figure 7C)**. As a results, $ZnFe_2O_4$ NCs/rGO/GCE shows the good selectivity, stability, repeatability and reproducibility towards the detection of 4-NQ.

3.8. Real sample analysis

The practicality of the $ZnFe_2O_4$ NCs/rGO/GCE modified electrode was investigated DPV method. The real sample of human serum and urine samples were collected from the medical hospital (Taipei). Prior to the analysis, the human serum and urine samples were diluted with buffer and spiked with known concentration of 4-NQ by using the standard addition method. Later, the real samples were used to explore the practicality of the proposed sensor. DPV responses for the addition of human serum and urine samples spiked with 100 nM, 200 nM and 500 nM concentration of 4-NQ. Then, the peak current responses were

increased for each addition of 4-NQ spiked samples. The obtained peak current responses have calculated against the concentration. Moreover, the RSD (n=3) results were calculated and tabulated in **Table 1**. It can be seen that the appreciable recovery results were obtained for the determination of 4-NQ in human serum and urine samples.

Table 1. Determination of 4-NQ in real samples based on $ZnFe_2O_4$ NCs/rGO/GCE

Real Samples	Added/nM	Found/nM	Recovery/%	*RSD/%
Blood serum	0	-	-	-
	100	98.36	98.36	3.68
	200	188.23	94.11	3.37
	500	491.35	98.27	3.71
Urine	0	-	-	-
	100	95.91	95.91	3.26
	200	191.34	95.67	3.48
	500	484.32	96.86	3.35

* Related standard deviation (RSD) of n=3 independent experiments.

4. Conclusion

In summary, the $ZnFe_2O_4$ NCs decorated rGO was synthesized by facile sonochemical method. Further, the resultant nanomaterial was characterized through the appropriate spectrophotometric techniques including HR-TEM, XRD, XPS, EIS and CV. As-prepared $ZnFe_2O_4$ NCs/rGO nanocomposite was used to fabricate the modified GCE for the

determination biomarker. The electrocatalytic activity of the $ZnFe_2O_4$ NCs/rGO/GCE for the detection of 4-NQ was evaluated using CV and DPV methods. Furthermore, the DPV study reveals the wide linear range 0.025-534.12 µM and the LOD is 8.27 nM towards the determination of 4-NQ. Besides, the interference study proved that our proposed sensor has good selectivity towards the detection of 4-NQ. Mainly, our proposed sensor $ZnFe_2O_4$ NCs/rGO nanomaterial exhibited an excellent stability and reproducibility. Furthermore, we have successfully demonstrated the practical ability of the 4-NQ sensor in human blood and urine samples.

Acknowledgments

The authors extend their appreciation to the International Scientific Partnership Program ISPP at King Saud University for funding this research work through ISPP# 0045. This project was also supported by the Ministry of Science and Technology (MOST 107-2113-M-027-005-MY3), Taiwan (ROC).

References

[1] J. Li, Q. Meng, Y. Zhang, L. Peng, G. Yu, A.C. Marschilok, L. Wu, D. Su, K.J. Takeuchi, E.S. Takeuchi, Size-dependent kinetics during non-equilibrium lithiation of nano-sized zinc ferrite, Nature communications, 10 (2019) 93.

[2] S. Gupta, C. Chang, C.-H. Lai, N.-H. Tai, Hybrid composite mats composed of amorphous carbon, zinc oxide nanorods and nickel zinc ferrite for tunable electromagnetic interference shielding, Composites Part B: Engineering, 164 (2019) 447-457.

[3] M.S. Javed, Z. Jiang, Q. Yang, X. Wang, X. Han, C. Zhang, X. Gu, C. Hu, Exploring Li-ion hopping behavior in zinc ferrite and promoting performance for flexible solid-state supercapacitor, Electrochimica Acta, 295 (2019) 558-568.

[4] Q. Zhang, Z. Li, X. Li, L. Yu, Z. Zhang, Z. Wu, Zinc ferrite nanoparticle decorated boron nitride nanosheet: Preparation, magnetic field arrangement, and flame retardancy, Chemical Engineering Journal, 356 (2019) 680-692.

[5] L. Yang, C. Sun, H. Lin, X. Gong, T. Zhou, W.-T. Deng, Z. Chen, J. Gao, Sensitive Contrast-Enhanced MR Imaging of Orthotopic and Metastatic Hepatic Tumors by Ultralow Doses of Zinc Ferrite Octapods, Chemistry of Materials, (2019).

[6] K. Sakthivel, G. Mani, S.-M. Chen, S.-H. Lin, A. Muthumariappan, V. Mani, A novel synthesis of non-aggregated spinel nickel ferrite nanosheets for developing non-enzymatic reactive oxygen species sensor in biological samples, Journal of Electroanalytical Chemistry, 820 (2018) 161-167.

[7] S.-M. Chen, R. Umamaheswari, G. Mani, T.-W. Chen, M.A. Ali, A.-H. Fahad, M. Elshikh, M.A. Farah, Hierarchically structured CuFe 2 O 4 ND@ RGO composite for the detection of oxidative stress biomarker in biological fluids, Inorganic Chemistry Frontiers, 5 (2018) 944-950.

[8] S. Kogularasu, M. Govindasamy, S.-M. Chen, M. Akilarasan, V. Mani, 3D graphene oxide-cobalt oxide polyhedrons for highly sensitive non-enzymatic electrochemical determination of hydrogen peroxide, Sensors and Actuators B: Chemical, 253 (2017) 773-783.

[9] M. Govindasamy, S. Shanthi, E. Elaiyappillai, S.-F. Wang, P.M. Johnson, H. Ikeda, Y. Hayakawa, S. Ponnusamy, C. Muthamizhchelvan, Fabrication of hierarchical NiCo2S4@ CoS2 nanostructures on highly conductive flexible carbon cloth substrate as a hybrid electrode material for supercapacitors with enhanced electrochemical performance, Electrochimica Acta, 293 (2019) 328-337.

[10] M. Govindasamy, S. Manavalan, S.-M. Chen, R. Umamaheswari, T.-W. Chen, Determination of oxidative stress biomarker 3-nitro-L-tyrosine using CdWO4 nanodots decorated reduced graphene oxide, Sensors and Actuators B: Chemical, 272 (2018) 274-281.

[11] S. Manavalan, M. Govindasamy, S.-M. Chen, U. Rajaji, T.-W. Chen, M.A. Ali, F.M. Al-Hemaid, M. Elshikh, M.A. Farah, Reduced graphene oxide supported raspberry-like SrWO4 for sensitive detection of catechol in green tea and drinking water samples, Journal of the Taiwan Institute of Chemical Engineers, 89 (2018) 215-223.

[12] T.-W. Chen, U. Rajaji, S.-M. Chen, M. Govindasamy, S.S.P. Selvin, S. Manavalan, R. Arumugam, Sonochemical synthesis of graphene oxide sheets supported Cu2S nanodots for high sensitive electrochemical determination of caffeic acid in red wine and soft drinks, Composites Part B: Engineering, 158 (2019) 419-427.

[13] M. Govindasamy, S.-F. Wang, S. Kumaravel, R.J. Ramalingam, H.A. Al-lohedan, Facile synthesis of copper sulfide decorated reduced graphene oxide nanocomposite for high sensitive detection of toxic antibiotic in milk, Ultrasonics sonochemistry, (2018).

[14] M.H. Sousa, F.A. Tourinho, J. Depeyrot, G.J. da Silva, M.C.F. Lara, New electric double-layered magnetic fluids based on copper, nickel, and zinc ferrite nanostructures, The Journal of Physical Chemistry B, 105 (2001) 1168-1175.

[15] V. Mani, B. Devadas, S.-M. Chen, Direct electrochemistry of glucose oxidase at electrochemically reduced graphene oxide-multiwalled carbon nanotubes hybrid material modified electrode for glucose biosensor, Biosensors and Bioelectronics, 41 (2013) 309-315.

[16] V. Mani, B. Dinesh, S.-M. Chen, R. Saraswathi, Direct electrochemistry of myoglobin at reduced graphene oxide-multiwalled carbon nanotubes-platinum nanoparticles nanocomposite and biosensing towards hydrogen peroxide and nitrite, Biosensors and Bioelectronics, 53 (2014) 420-427.

[17] R. Devasenathipathy, V. Mani, S.-M. Chen, Highly selective amperometric sensor for the trace level detection of hydrazine at bismuth nanoparticles decorated graphene nanosheets modified electrode, Talanta, 124 (2014) 43-51.

[18] B. Unnikrishnan, V. Mani, S.-M. Chen, Highly sensitive amperometric sensor for carbamazepine determination based on electrochemically reduced graphene oxide–single-walled carbon nanotube composite film, Sensors and Actuators B: Chemical, 173 (2012) 274-280.

[19] V. Mani, R. Devasenathipathy, S.-M. Chen, S.-F. Wang, P. Devi, Y. Tai, Electrodeposition of copper nanoparticles using pectin scaffold at graphene nanosheets

for electrochemical sensing of glucose and hydrogen peroxide, Electrochimica Acta, 176 (2015) 804-810.

[20] M. Govindasamy, S.-F. Wang, W.C. Pan, B. Subramanian, R.J. Ramalingam, H. Al-lohedan, Facile Sonochemical Synthesis of Perovskite-Type $SrTiO_3$ Nanocubes with Reduced Graphene Oxide Nanocatalyst for an Enhanced Electrochemical Detection of α-Amino Acid (Tryptophan), Ultrasonics Sonochemistry, (2019).

[21] M. Govindasamy, B. Subramanian, S.-F. Wang, S. Chinnapaiyan, R.J. Ramalingam, H. Al-lohedan, Ultrasound-Assisted Synthesis of Tungsten Trioxide Entrapped with Graphene Nanosheets for Developing Nanomolar Electrochemical (Hormone) Sensor and Enhanced Sensitivity of the Catalytic Performance, Ultrasonics Sonochemistry, (2019).

[22] M. Govindasamy, R. Umamaheswari, S.-M. Chen, V. Mani, C. Su, Graphene oxide nanoribbons film modified screen-printed carbon electrode for real-time detection of methyl parathion in food samples, Journal of The Electrochemical Society, 164 (2017) B403-B408.

[23] V. Mani, T.-W. Chen, S. Selvaraj, MWCNTs/MoS_2 Decorated Cobalt Oxide Polyhedrons Composite Film Modified Electrode for Electrochemical Determination of Dopamine in Rat Brain and Human Blood Serum Samples, Int. J. Electrochem. Sci, 12 (2017) 7435-7445.

[24] M. Govindasamy, S.-M. Chen, V. Mani, M. Akilarasan, S. Kogularasu, B. Subramani, Nanocomposites composed of layered molybdenum disulfide and graphene for highly sensitive amperometric determination of methyl parathion, Microchimica Acta, 184 (2017) 725-733.

[25] V. Mani, M. Govindasamy, S.-M. Chen, B. Subramani, A. Sathiyan, J.P. Merlin, Determination of folic acid using graphene/molybdenum disulfide nanosheets/gold nanoparticles ternary composite, Int. J. Electrochem. Sci, 12 (2017) e267.

[26] V. Mani, M. Govindasamy, S.-M. Chen, T.-W. Chen, A.S. Kumar, S.-T. Huang, Core-shell heterostructured multiwalled carbon nanotubes@ reduced graphene oxide nanoribbons/chitosan, a robust nanobiocomposite for enzymatic biosensing of hydrogen peroxide and nitrite, Scientific reports, 7 (2017) 11910.

[27] M. Govindasamy, V. Mani, S.-M. Chen, T. Maiyalagan, S. Selvaraj, T.-W. Chen, S.-Y. Lee, W.-H. Chang, Highly sensitive determination of non-steroidal anti-inflammatory drug nimesulide using electrochemically reduced graphene oxide nanoribbons, RSC Advances, 7 (2017) 33043-33051.

[28] T. Nunoshiba, B. Demple, Potent intracellular oxidative stress exerted by the carcinogen 4-nitroquinoline-N-oxide, Cancer Research, 53 (1993) 3250-3252.

[29] M. Govindasamy, S.-M. Chen, V. Mani, A. Sathiyan, J.P. Merlin, F.M. Al-Hemaid, M.A. Ali, Simultaneous determination of dopamine and uric acid in the presence of high ascorbic acid concentration using cetyltrimethylammonium bromide–polyaniline/activated charcoal composite, RSC Advances, 6 (2016) 100605-100613.

[30] M. Govindasamy, V. Mani, S.-M. Chen, T.-W. Chen, A.K. Sundramoorthy, Methyl parathion detection in vegetables and fruits using silver@graphene nanoribbons nanocomposite modified screen printed electrode, Scientific reports, 7 (2017) 46471.

[31] J. Zheng, T. Gao, H. Shi, Y. Huang, Y. Xiang, G. Li, Electrochemical analysis of 8-hydroxy-2’-deoxyguanosine with enhanced sensitivity based on exonuclease-mediated functional nucleic acid, Talanta, (2019).

[32] A.R. Khandelwal, T. Moore-Medlin, O. Ekshyyan, X. Gu, F. Abreo, C.-A.O. Nathan, Local and systemic Curcumin C3 complex inhibits 4NQO-induced oral tumorigenesis via modulating FGF-2/FGFR-2 activation, American Journal of Cancer Research, 8 (2018) 2538.

[33] Y.C. Fann, C.A. Metosh-Dickey, G.W. Winston, A. Sygula, D. Ramakrishna Rao, M.B. Kadiiska, R.P. Mason, Enzymatic and nonenzymatic production of free radicals from the carcinogens 4-nitroquinoline N-oxide and 4-hydroxylaminoquinoline N-oxide, Chemical research in toxicology, 12 (1999) 450-458.

[34] S. Kailasam, K. Rogers, A fluorescence-based screening assay for DNA damage induced by genotoxic industrial chemicals, Chemosphere, 66 (2007) 165-171.

[35] F. Blasi, L. Dominici, M. Moretti, M. Villarini, S. Maurelli, M.S. Simonetti, P. Damiani, L. Cossignani, In vitro genotoxicity/antigenotoxicity testing of some conjugated linoleic acid isomers using comet assay, European journal of lipid science and technology, 114 (2012) 1016-1024.

[36] I. Bobeldijk, A. Brandt, B. Wullings, T. Noij, High-performance liquid chromatography–ToxPrint: chromatographic analysis with a novel (geno) toxicity detection, Journal of Chromatography A, 918 (2001) 277-291.

[37] S.-M. Chen, S. Manavalan, U. Rajaji, M. Govindasamy, T.-W. Chen, M.A. Ali, A.K. Alnakhli, F.M. Al-Hemaid, M. Elshikh, Determination of the antioxidant propyl gallate in meat by using a screen-printed electrode modified with $CoSe_2$ nanoparticles and reduced graphene oxide, Microchimica Acta, 185 (2018) 520.

[38] M. Govindasamy, S. Manavalan, S.-M. Chen, U. Rajaji, T.-W. Chen, F.M. Al-Hemaid, M.A. Ali, M.S. Elshikh, Determination of Neurotransmitter in Biological and Drug Samples Using Gold Nanorods Decorated f-MWCNTs Modified Electrode, Journal of The Electrochemical Society, 165 (2018) B370-B377.

[39] M. Govindasamy, V. Mani, S.-M. Chen, A. Sathiyan, J.P. Merlin, G. Boopathy, Polyaniline/nickel Composite Film Modified Electrode for Sensitive Electrochemical Determination of Ascorbic Acid, International Journal of Electrochemical Science, 11 (2016) 10806-10814.

[40] M. Govindasamy, V. Mani, S.-M. Chen, B. Subramani, R. Devasenathipathy, S. Tamilarasan, Highly Sensitive Amperometric Sensor for Nitrobenzene Detection Using Functionalized Multiwalled-Carbon Nanotubes Modified Screen Printed Carbon Electrode, International Journal of Electrochemical Science, 11 (2016) 10837-10846.

[41] M. Govindasamy, U. Rajaji, S.-M. Chen, S. Kumaravel, T.-W. Chen, F.M. Al-Hemaid, M.A. Ali, M.S. Elshikh, Detection of pesticide residues (Fenitrothion) in fruit samples based on niobium carbide@ molybdenum nanocomposite: an electrocatalytic approach, Analytica chimica acta, 1030 (2018) 52-60.

[42] V. Mani, A.P. Periasamy, S.-M. Chen, Highly selective amperometric nitrite sensor based on chemically reduced graphene oxide modified electrode, Electrochemistry Communications, 17 (2012) 75-78.

[43] V. Mani, S. Shanthi, T.-K. Peng, H.-Y. Lin, H. Ikeda, Y. Hayakawa, S. Ponnusamy, C. Muthamizhchelvan, S.-T. Huang, Real-time quantification of hydrogen peroxide production in living cells using $NiCo_2S_4$@CoS_2 heterostructure, Sensors and Actuators B: Chemical, (2019).

[44] G. Boopathy, M. Keerthi, S.-M. Chen, M. Umapathy, M. Govindasamy, T.-W. Chen, M.A. Ali, F.M. Al-Hemaid, M. Elshikh, Graphene Oxide/α-MnO_2 Binary Nanosheets Based Non-Enzymatic Biosensor for Pico-Molar Level Electrochemical Detection of Biomarker (Guanine) in DNA Sample, Journal of The Electrochemical Society, 165 (2018) B651-B658.

[45] F. Liu, X. Chu, Y. Dong, W. Zhang, W. Sun, L. Shen, Acetone gas sensors based on graphene-$ZnFe_2O_4$ composite prepared by solvothermal method, Sensors and Actuators B: Chemical, 188 (2013) 469-474.

[46] C.-H. Chen, Y.-H. Liang, W.-D. Zhang, $ZnFe_2O_4$/MWCNTs composite with enhanced photocatalytic activity under visible-light irradiation, Journal of Alloys and Compounds, 501 (2010) 168-172.

[47] P. Uniyal, K. Yadav, Synthesis and study of multiferroic properties of $ZnFe_2O_4$–$BiFeO_3$ nanocomposites, Journal of Alloys and Compounds, 492 (2010) 406-410.

[48] S. Manavalan, U. Rajaji, S.-M. Chen, M. Govindasamy, S.S.P. Selvin, T.-W. Chen, M.A. Ali, F.M. Al-Hemaid, M. Elshikh, Sonochemical synthesis of bismuth (III) oxide decorated reduced graphene oxide nanocomposite for detection of hormone (epinephrine) in human and rat serum, Ultrasonics sonochemistry, 51 (2019) 103-110.

[49] U. Rajaji, K. Murugan, S.-M. Chen, M. Govindasamy, T.-W. Chen, P.H. Lin, Graphene oxide encapsulated 3D porous chalcopyrite ($CuFeS_2$) nanocomposite as an emerging electrocatalyst for agro-hazardous (methyl paraoxon) detection in vegetables, Composites Part B: Engineering, 160 (2019) 268-276.

[50] T.-W. Chen, U. Rajaji, S.-M. Chen, R.J. Ramalingam, A relative study on sonochemically synthesized mesoporous WS_2 nanorods & hydrothermally synthesized WS2 nanoballs towards electrochemical sensing of psychoactive drug (Clonazepam), Ultrasonics sonochemistry, (2019).

Research Highlights

1) Facile sonochemical synthesis of Bimetal ferrite catalyst (BFC) based zinc ferrite nanocubes decorated on multi-layered reduced graphene oxide ($ZnFe_2O_4$ NCs/rGO) nanocomposite have been developed.

2) The $ZnFe_2O_4$ NCs/rGO nanocomposite was applied to the electrochemical sensor.
3) The $ZnFe_2O_4$ NCs/rGO has detected nanomolar level with broad dynamic range towards 4-NQ.
4) The nanocomposite of $ZnFe_2O_4$ NCs/rGO was successfully applied real sample analysis.